Favorable Intercalation of Nitrate Ions with Fluorine-Substituted Layered Double Hydroxides

Tomohito Sudare, Marc Dubois, Nicolas Louvain, Masahiro Kiyama, Fumitaka Hayashi, Katsuya Teshima

Inorganic Chemistry
Cite This: Inorg. Chem. XXXX, XXX, XXX–XXX
Article
pubs.acs.org/IC

Favorable Intercalation of Nitrate Ions with Fluorine-Substituted Layered Double Hydroxides

Tomohito Sudare,[†] Marc Dubois,[§] Nicolas Louvain,[∥,⊥] Masahiro Kiyama,[‡] Fumitaka Hayashi,[‡] and Katsuya Teshima*[,†,‡]

[†]Research Initiative for Supra-Materials, Shinshu University, Nagano 380-8553, Japan
[‡]Department of Materials Chemistry, Shinshu University, Nagano 380-8553, Japan
[§]Université Clermont Auvergne, SIGMA Clermont, UMR CNRS 6296, 24 avenue des Blaise Pascal, 63178 Aubière, France
[∥]Institut Charles Gerhardt Montpellier, Université de Montpellier, CNRS, 34090 Montpellier, France
[⊥]Réseau sur le Stockage Electrochimique de l'Energie (RS2E), FR CNRS 3459, 33 Rue Saint Leu, 80039 Amiens, France

Supporting Information

ABSTRACT: Understanding and controlling confined nanospace to accommodate substrates and promote high ion conduction are essential to various fields. Layered double hydroxides (LDHs) have emerged as promising candidates for anion exchangers using the interlayer nanospace in their crystal structures. Miyata reported in 1983 that the affinity of anions for intercalation with most major Mg−Al LDHs increased in the following order: NO_3^- < Br^- < F^- < SO_4^{2-} < HPO_3^{2-}. Attempts to alter the affinity with different metal cations (M^{2+} and M^{3+}) have been unsuccessful. Analyses of the crystalline structures of LDHs, positively charged host layers, interlayer anions, and interlayer water molecules indicate that they inevitably interact through hydrogen bonding. In other words, the affinity of LDHs for anions is controlled by tuning the hydrogen bonding. In this study, we prepared fluorine-substituted LDHs (F-LDHs) with different Mg/Al ratios by partially replacing the OH structural groups, which originated from the host layer, with fluorine atoms; the resulting change in affinity was investigated. The distribution coefficient, which is a useful indicator of the affinity of an LDH for a particular anion, was examined. The results showed that only F-LDHs with Mg/Al ratios of 3.5 exhibited high affinity, especially for NO_3^- ions, and the affinity increased in the following order: HPO_4^{2-} < SO_4^{2-} < F^- < Br^- < NO_3^-. The separation factors of these specific F-LDHs with respect to both NO_3^-/F^- and NO_3^-/SO_4^{2-} were higher than that of LDHs with other compositions by 1 order of magnitude. Raman spectroscopy above 3000 cm^{-1} revealed that the fluorine substitution of LDHs significantly changed the hydrogen bonding nature in the interlayer space. Highly electronegative fluorine atoms significantly decrease the extent of hydrogen bonding interactions between OH structural groups and both interlayer water molecules and anions, wherein steric effects are induced by the shrunken interlayer space, and van der Waals forces are revealed to be the predominant interaction with anions. Therefore, the highest affinity was observed for NO_3^- ions in F-LDHs.

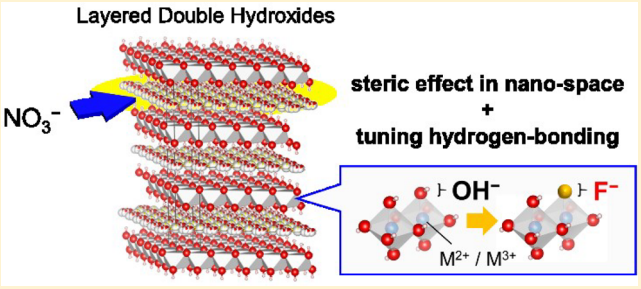

INTRODUCTION

Various unique materials with confined nanospaces such as carbon, metal organic frameworks/porous coordination polymers, zeolites, and inorganic crystalline materials have been studied to understand and control the confined nanospace in their structure, to accommodate substrates, and to promote high ion conduction.[1−3] Layered double hydroxides (LDHs) are regarded as attractive sustainable photo- and electrocatalysts and ion exchangers due to their unique two-dimensional layer structure composed of various transition metals and their ability to accommodate anionic species in the interlayer space.[4−16] They are represented by the general formula $[M^{2+}_{1-x}M^{3+}_{x}(OH)_2]^{x+}[A^{n-}]_{x/n}\cdot mH_2O$ and consist of octahedral brucite-like layers (containing divalent and trivalent metal cations, M^{2+} and M^{3+}), charge-balancing interlayer anions (A^{n-}), and interlayer water molecules with rhombohedral symmetry (space group $R\bar{3}m$). Possible M^{2+} species are Mg^{2+}, Ni^{2+}, Zn^{2+}, Ca^{2+}, etc., and possible M^{3+} species are Al^{3+}, Cr^{3+}, Fe^{3+}, Co^{3+}, etc. The exchangeable anion, A^{n-}, can be either monovalent, such as OH^-, F^-, Cl^-, or NO_3^-, or divalent, such as SO_4^{2-}, HPO_4^{2-}, or CO_3^{2-}. Typically, a large amount of CO_3^{2-} ions with a relatively high charge density prefer to be contained in the interlayer space. In fact, LDHs have been useful for the removal of harmful oxo-anions (SO_4^{2-}, HPO_4^{2-}, NO_3^-, etc.) from environmental water because of their capacious interlayer space.

Received: May 26, 2019

DOI: 10.1021/acs.inorgchem.9b01552
Inorg. Chem. XXXX, XXX, XXX–XXX

The presence of nitrate and nitrous ions in groundwater has become a serious concern worldwide in recent decades.[17,18] For example, babies can suffer from blue baby syndrome caused by polluted drinking water. Compared to other anions like F^-, Br^-, I^-, SO_4^{2-}, and HPO_3^{2-}, NO_3^- ions are delocalized and have a low charge density, which make them difficult to capture by conventional adsorbents owing to their electrostatic interaction with the adsorbent used. Therefore, it is of great scientific interest to increase the affinity of a selected captor for NO_3^- ions.

The ion-exchange capability, selectivity, and capacity of LDHs have been widely studied. Miyata previously reported that the affinity of most well-known Mg−Al LDHs for various anions increases in the following order: $NO_3^- < Br^- < Cl^- < F^- < OH^- < MoO_4^{2-} < SO_4^{2-} < CrO_4^{2-} < HAsO_3^{2-} < HPO_3^{2-} < CO_3^{2-}$.[3] Costa et al. reported that the order of exchange selectivity based on a computational simulation for Zn−Al LDHs (Zn/Al = 2) is as follows: $NO_3^- < Br^- < CO_3^{2-} < Cl^- < F^- < OH^-$.[19] Puerta-Falla et al. reported that the affinity of Ca−Al LDH for anions increases in the following order: $OH^- < SO_4^{2-} < CO_3^{2-} < Cl^- < NO_2^- < NO_3^-$. However, LDHs of this composition can be used only under alkaline conditions.[7] It has been shown that LDHs show a higher affinity for anions with a higher charge density. It is important to note that NO_3^- ions are intrinsically the most difficult anions to capture from water, even by using LDHs. There are many informative reports on the relationship between the chemical composition of LDHs and their affinity for anions, such as the combination of M^{2+} and M^{3+} species and the M^{2+}/M^{3+} ratio in a brucite-like layer, and the orientation and diffusion coefficients of interlayer anions.[20−22] For example, it was reported that the charge density in the brucite-like layer of an LDH significantly affects the amount of water contained in the interlayer space, leading to a change in the orientation of interlayer NO_3^- ions.[18,19] In the case of Zn−Al LDHs, the diffusion coefficient in the interlayer space is higher than those in the interlayer space of Zn−Ga, Mg−Al, and Mg−Ga LDHs.[20] However, the key factor to determine the order of affinity under actual ion-exchange conditions remains unclear. Careful observation of the crystal structure of LDHs revealed that the interlayer anions and water molecules intrinsically lie at comfortable positions in the interlayer space by interacting through hydrogen bonding with OH structural groups belonging to the brucite-like layers. In other words, the interlayer potential energy structure is controlled by not only the charge density but also the local intermolecular interactions with OH structural groups, which lead to our proposed strategy of substituting other elements for OH structural groups to tune the affinity of LDHs for NO_3^- ions. An OH structural group is monovalent and so small that fluorine is the best candidate for substituting it in a brucite-like layer in the viewpoint of thermodynamic stability (see Figure 1). Results from an earlier report have encouraged us to prepare fluorine-substituted LDHs (F-LDHs).[23] In this work, F-LDHs were successfully prepared by co-precipitation, and the effect of fluorine substitution on the basicity of LDHs was investigated. As the focus of their study was different, they did not try to control the chemical composition, crystallinity, or especially interlayer structure. In our study, we prepared F-LDHs composed of Mg and Al, and the effects of fluorine substitution on the affinity of these F-LDHs for various anions with different charge densities and molecular structures were comparatively studied using fluoride, nitrate, and sulfate ions as models (see Figure 1).

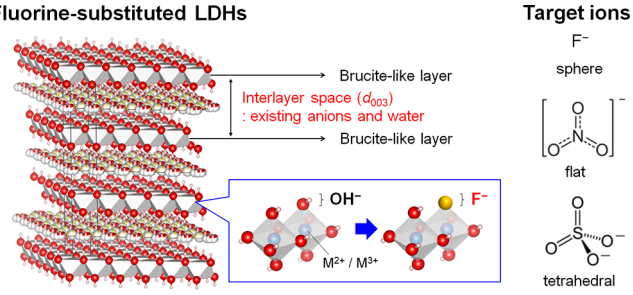

Figure 1. Crystal structure and schematic image of fluorine substitution of a brucite-like layer of LDHs, visualized using the VESTA program and molecular structures of the target ion in this study.

RESULTS AND DISCUSSION

Na_3AlF_6 was used as the fluorine precursor to prepare F-LDHs. In a typical synthesis procedure, the $[AlCl_3]/[Na_3AlF_6]$ ratio in the precursor solution was fixed at 1.0, and the $([AlCl_3] + [Na_3AlF_6])/[MgCl_2]$ ratio was varied in the range of 2.5−4.0 to control the Mg/Al ratio in the products. Hereafter, the samples were labeled according to the chemical composition, where 35 and 35F, for example, refer to LDHs without and with fluorine substitution, respectively, whose targeted Mg/Al ratio was 3.5. The representative scanning electron microscopy (SEM) images of two prepared LDHs, 35 and 35F, after Cl^--exchange treatment are shown in panels a and b of Figure 2.

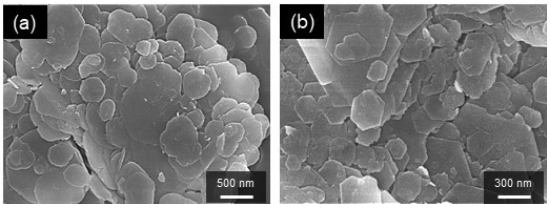

Figure 2. FE-SEM images of (a) 35 and (b) 35F after Cl-exchange treatment.

Plate-shaped particles with sizes in the range of 100−500 nm were obtained in both samples. The surfaces of these particles were partially connected to each other, and these connections might have formed during crystallization of the as-prepared LDH agglomerates by co-precipitation. In 35F, most LDH particles had clearly defined hexagonal shapes as shown in Figure 2b, although particles with round shapes were observed in 35 as shown in Figure 2a, possibly because the free fluoride ions released in 35F from the precursor Na_3AlF_6 worked as a structure-guiding agent or mineralizer, or both. It is important to note here that the complexation state of Na_3AlF_6 is known to change depending on the pH of the solution. It was reported that most of the Na_3AlF_6 releases fluoride ions to form $[Al(OH)_{4-x}F_x]^-$ in an aqueous solution at pH >10 and 50 °C.[24] This means that fluoride ions and partially fluorinated hydroxy aluminum ions coexisted in the reaction solution during co-precipitation as proposed in eq 1, where $g = a(4 - c)$, and the fluoride ions worked as a structure-guiding agent or mineralizer (or both), while the partially fluorinated hydroxy aluminum ions worked as a fluorine source in the brucite-like layer of an LDH. It should also be noted that the change in

DOI: 10.1021/acs.inorgchem.9b01552
Inorg. Chem. XXXX, XXX, XXX−XXX

complexation state possibly limited the amount of fluorine substitution in the resulting LDH particles.

$$(1 - a - b)Mg^{2+} + a[Al(OH)_cF_{4-c}]^- + bAl^{3+} + dOH^- + [(a + b)/2]CO_3^{2-} + eH_2O \rightarrow [Mg_{1-a-b}Al_{a+b}(OH)_{2-f}F_f][(a + b)/2]CO_3^{2-}\cdot eH_2O + (g - f)F^- \quad (1)$$

The XRD patterns of all samples after Cl^--exchange treatment are shown in Figure 3, with an enlarged view of

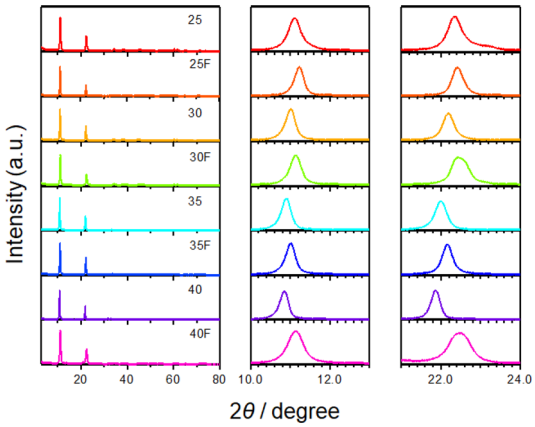

Figure 3. XRD patterns of F-LDH and original LDHs after Cl-exchange treatment.

the region in the 2θ range of 11−22°. With the exception of 40F, LDH was successfully formed in all samples without distinct byproducts, even after the Cl^--exchange treatment. The XRD patterns also reveal two different trends in the position of diffraction lines: the (003) line at 2θ of ∼11°, which corresponds to the basal spacing of two neighboring brucite-like layers (d_{003}); the (006) diffraction line around 22°, which corresponds to the basal spacing between the interlayer anion layer and the brucite-like layer (d_{006}) (see Figure 1a). First, d_{003} and d_{006} increased with an increase in the Mg/Al ratio in the LDHs. For example, d_{003} increased from 7.96 Å in 25 (Mg/Al = 2.5) to 8.12 Å in 35 (Mg/Al = 3.5), suggesting that the lower charge density of the brucite-like layer led to weaker interaction with the interlayer anions and water molecules, resulting in expansion of the interlayer distance. Second, d_{003} and d_{006} slightly decreased as a result of fluorine substitution in samples with the same Mg/Al ratio, such as 35 and 35F (Mg/Al = 3.5). For example, d_{003} had values of 8.12 Å in 35 and 8.03 Å in 35F, which also imply that the brucite-like layers strongly interacted with the interlayer anions and water molecules in the F-LDHs when compared with the interaction in the original LDHs. These results indicate that the interlayer potential structure of LDHs can be tuned by adjusting the chemical composition of both cation and anion species belonging to the brucite-like layers.

Next, the incorporation of fluorine atoms into the brucite-like layers of LDHs was confirmed by solid-state magic angle spinning nuclear magnetic resonance (MAS NMR) (Figure 4). Data for both ^{27}Al and ^{19}F nuclei highlight the absence of residual Na_3AlF_6. Resonance lines of Na_3AlF_6 are expected at −0.8 ppm[25] (vs 1.0 M aqueous $AlCl_3$) and −189 ppm[26] (vs $CFCl_3$) for their ^{27}Al and ^{19}F NMR spectra, respectively, and these lines are absent for both 35F and 40F samples (Figure

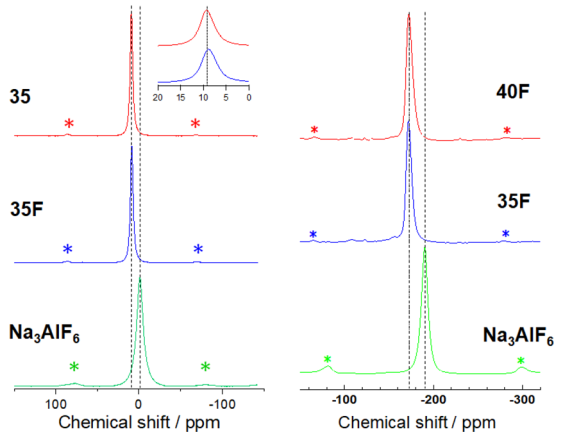

Figure 4. ^{27}Al solid-state nuclear magnetic resonance spectra of LDHs [35 in red, 35F in blue, and Na_3AlF_6 in green (left)] and ^{19}F solid-state nuclear magnetic resonance spectra of LDHs [40F in red, 35F in blue, and Na_3AlF_6 in green (right)]. *, satellite signals.

4). The chemical shift for ^{19}F in Na_3AlF_6 is −190 ppm, which is in good accordance with the reported data. For both ^{27}Al and ^{19}F NMR experiments, 35, 35F, and 40F samples showed similar results, most probably indicating similar local environments for Al and F atoms in each material, and appear to be shifted in comparison with those in Na_3AlF_6. The ^{19}F chemical shift for 35F and 40F is −172 ppm, a value close to that reported for AlF_3 ($\delta_{^{19}F}$ = −170 ppm[27−30]). It can thus be concluded that the F atom environment in 35F and 40F samples should be like that found in AlF_3 (see Figure S1), which is a fluorine atom surrounded by two aluminums. It is important to remember that AlF_3 crystallizes in rhombohedral space group $R\bar{3}c$ and it is isostructural with a distorted ReO_3-type structure, analogous to an A-site deficient perovskite which consists of corner-sharing AlF_6 octahedra.[31] The situation is different for the ^{27}Al spectra. The NMR peak of both 35 and 35F appears at 8.84 ppm, shifted from the expected $\delta_{^{27}Al}$ value of −15.9 ppm for AlF_3.[27] This highlights the presence of neighboring oxygen atoms in the vicinity of the Al atoms. As a comparison, it should be considered that aluminum atoms in solid alkali fluoroaluminates are essentially coordinated with six fluorine atoms in an octahedral geometry, and their reported ^{27}Al chemical shifts lie between −15 and +1.4 ppm, which is approximately 20 ppm more shielded than that of AlO_6 octahedra in aluminum oxides.[32−34] It is noteworthy that MgF_2 is not formed during the fluorination of LDH samples, as its ^{19}F chemical shift (−196 ppm[35]) is not detected in any spectrum (Figure 4).

It seems reasonable to assume that Al environments in 35F and 40F are composed of both fluorine and oxygen atoms,[36,37] while the vicinity of fluorine is populated with aluminum atoms.

For quantitative measurements, polytetrafluoroethylene (PTFE) was added to the rotor as an internal reference (Figure S2). The fluorine content of 40F was determined to be 1.43 times higher than that of 35F, which is in good accordance with the results of EDS analysis [1.50, i.e., F/(OH + F) ratios of 0.10 and 0.15 for 35F and 40F, respectively (Table S1)].

The chemical composition of each LDH was analyzed by EDS and ICP-OES; the results are summarized in Table. S1. The different Mg/Al ratios among the products were approximately controlled by changing the target precursor

DOI: 10.1021/acs.inorgchem.9b01552
Inorg. Chem. XXXX, XXX, XXX−XXX

concentration used during sample preparation. The ratio of fluorine substitution for structural hydroxyl groups was calculated using F/2(Mg + Al), with the elemental concentrations analyzed by EDS; this ratio was found to be limited to <10% in all F-LDHs. For these calculations, we assumed that almost all residual fluoride ions in the interlayer were exchanged with chloride ions. More importantly, ~80% of the ion-exchange sites were occupied by chloride ions, and the residual sites were occupied by carbonate ions; the presence of carbonates in the interlayer was also confirmed by Fourier transform infrared (FT-IR) measurements, as described below. The included water was analyzed by TG-DTA measurements as shown in Figure S3. On the basis of the results of the analysis, the prepared LDHs, e.g., 35F and 35, can be described by the chemical formulas $[Mg_{0.77}Al_{0.23}(OH)_{1.82}F_{0.18}](Cl^-)_{0.15}\cdot(CO_3^{2-})_{0.04}\cdot 0.67H_2O$ and $[Mg_{0.77}Al_{0.23}(OH)_2](Cl^-)_{0.16}\cdot(CO_3^{2-})_{0.03}\cdot 0.63H_2O$, respectively.

The ion-exchange capability, i.e., affinity for a specific type of ions, was examined by focusing on the compatibility of the Mg/Al ratio and fluorine substitution in LDHs. First, the distribution coefficient (K_d) was evaluated; it is traditionally used as an indicator of the affinity of particular ions for the solid phase relative to the liquid phase. In general, it is difficult to obtain the precise concentration of a particular type of ion in a stoichiometric ion-exchange manner because multiple reactions can occur in an actual testing solution, such as physical or chemical (or both physical and chemical) adsorption on the surface and ion-exchange reactions with two or three types of ions. It is also unfortunate that conventional reports do not mention the stoichiometry of ion-exchange reactions involving LDHs. Generally, the concentration of particular ions from the testing solution permeating into an LDH in a stoichiometric manner should be in accordance with the concentration of ions released from the LDH to the testing solution. In our study, there were three types of anions in the testing solution: target anions, released chloride anions, and hydroxyl ions. Thus, the K_d values were calculated from the respective concentrations of the target anions, Cl^- ions measured by IC, and OH^- ions measured by the pH meter. It is noted that the pH value throughout the ion-exchange test was maintained at 5−6 without any intentional control. As shown in Figure 5a, the K_d values of the LDHs for F^- ions decreased depending on the Mg/Al ratio in both F-LDHs and original LDHs, and the lowest value of 781 mL g^{-1} was observed in 35F. Figure 5b shows the K_d values of the samples for NO_3^- ions, and the maximum K_d values of both F-LDHs and original LDHs were found at a Mg/Al ratio of 3.5; the maximum value of 2434 mL g^{-1} of 35F is 3−5 times the values of K_d of LDHs with other compositions. For samples with low Mg/Al ratios, the K_d values for NO_3^- ions were lower than those for F^- ions, which is in agreement with previously reported results. This difference in K_d values is acceptable because a higher charge density of F^- ions resulted in strong interaction with a brucite-like layer whose charge density is higher because of the low Mg/Al ratio of the LDH. Finally, the K_d values for SO_4^{2-} ions, shown in Figure 5c, exhibited two opposite trends in the case of F-LDHs and the original LDHs. Although similar K_d values were obtained for 25 and 25F, the K_d value of 35F significantly decreased to 574 mL g^{-1}. On the other hand, the K_d value of the original LDHs increased to 2597 mL g^{-1} for 30. In addition, we calculated the ratio between the measured concentration of anions after ion exchange and the total reduced concentration of anions. The ratios in all ion-exchange tests are shown as functions of the Mg/Al ratio in Figure S5. In almost all samples, ~80% of all of the anions were reduced via ion-exchange reactions. Remarkably, the ratio with respect to SO_4^{2-} ions was significantly lower for the F-LDHs, while the ratio with respect to NO_3^- ions was higher, which correspond to the results for K_d.

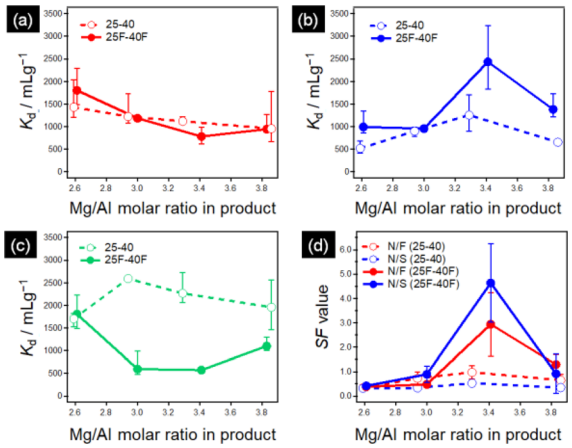

Figure 5. Dependence of the distribution coefficient (K_d) on Mg/Al ratio in (a) the F^--exchange test, (b) the NO_3^--exchange test, and (c) the SO_4^{2-}-exchange test. (d) Dependence of the separation factor on the Mg/Al ratio (*SF*).

To discuss the affinity more quantitatively, the separation factor (SF) was calculated (see Figure 5d). The $SF_{N/F}$ and $SF_{N/S}$ values were ~1.0 for all original LDHs, which means that their affinity for NO_3^- ions was lower than that for F^- and SO_4^{2-} ions. On the other hand, the $SF_{N/F}$ and $SF_{N/S}$ values of 35F are 5−10 times the corresponding values obtained for LDHs of other compositions. Furthermore, the trend of variation in affinity was systematically investigated for Br^-, I^-, and HPO_4^{2-} ions. The K_d values for Br^-, I^-, and HPO_4^{2-} ions were measured using 35 and 35F, and the K_d values are shown as functions of the ionic radius of the target anion in Figure S6. The affinity of the F-LDHs for divalent SO_4^{2-} and HPO_4^{2-} ions with large ionic radii was extremely low, and the affinity in the case of 35F increased in the following order: $HPO_4^{2-} < I^- < SO_4^{2-} < F^- < Br^- < NO_3^-$ (which implies specific size-recognizing behavior). Finally, the amount of fluorine substitution in the F-LDHs was controlled during the preparation process, and the dependence of $SF_{N/F}$ and $SF_{N/S}$ values on the amount of fluorine substitution was investigated. Both SF values were found to increase with an increased level of fluorine substitution, as shown in Figure S6. These results imply that the controlled combination of Mg/Al mixing at different ratios and fluorine substitution should be a key parameter to tune the interlayer structure of an LDH for improving its affinity of particular anions.

The size-recognizing behavior was related to the interlayer distance, the orientation of interlayer anions, and the structure of interlayer water. The interlayer distance after the ion-exchange test was studied by XRD analysis. Figure 6a shows XRD patterns in a selected 2θ range around the (003) and (006) diffraction patterns, where the blue lines indicate the position of the corresponding patterns before the ion-exchange test. After the F^--exchange test, the XRD pattern of most samples exhibited a slight shift toward higher 2θ values, which corresponds to a decrease in interlayer distance. For example,

DOI: 10.1021/acs.inorgchem.9b01552
Inorg. Chem. XXXX, XXX, XXX−XXX

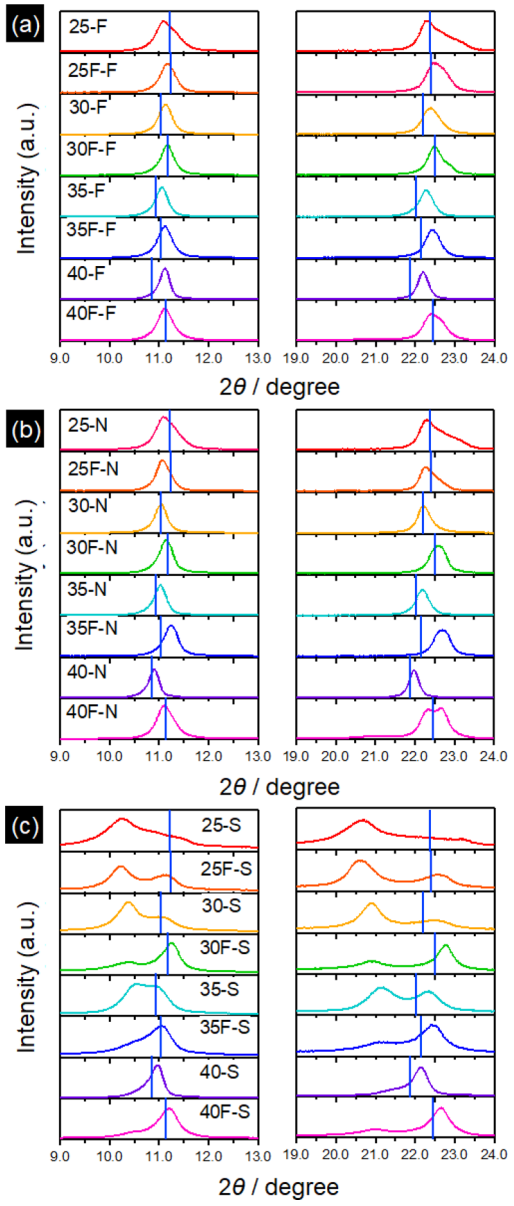

Figure 6. XRD patterns of LDHs after (a) the F^--exchange test, (b) the NO_3^--exchange test, and (c) the SO_4^{2-}-exchange test.

the interlayer distance decreased from 8.03 Å in 35 to 7.96 Å in 35F. This indicates the intercalation of F^- ions into the interlayer space of the LDH, leading to attractive forces between neighboring brucite-like layers. However, the change in interlayer distance after the F^--exchange test was small in all samples, suggesting that they contained smaller amounts of F^- ions in the LDH. Figure 6b shows the XRD patterns of all samples after the NO_3^--exchange test. The XRD patterns of 35, 35F, and 40F, however, exhibited larger shifts to higher 2θ, indicating a decreasing interlayer distance. The interlayer distance of 35F was 7.87 Å after the NO_3^- ion-exchange test and was found to be quite small among the samples. In particular, the (006) diffraction pattern offers information about the interlayer distance and orientation of interlayer anions. The (006) patterns of all F-LDHs were broader and positioned at 2θ values higher than those of the (006) pattern of the original LDHs, possibly because the interlayer NO_3^- ions had several types of orientations (e.g., vertical, parallel, and tilted) with respect to the brucite-like layer. For example, the interlayer NO_3^- ions in 35F had an approximately parallel orientation, because the thickness of a NO_3^- ion is 2.8 Å and the actual interlayer space calculated from the brucite layer thickness (4.8 Å) was 3.07 Å, although the interlayer distance of 8.03 Å in 35 implies that the NO_3^- ions were tilted from the brucite-like layer. An interesting result is that the interlayer distance of 7.87 Å in 35F after the NO_3^--exchange test is smaller than the interlayer distance of 7.96 Å after the F^--exchange test, even though the in-plane ionic radius of a NO_3^- ion is larger than that of a F^- ion. This finding suggests that before the ion-exchange test, F-LDH exhibited a shrunken interlayer space, and this trend is considered to be maintained, even after the test. This behavior indicates that steric effects are possibly induced in F-LDHs. In addition, the Mg/Al ratio should have been an important factor in the increased affinity observed in 35F. A higher Mg/Al ratio implies a lower number of interlayer anions in the interlayer space, leading to the strengthened steric and electrostatic repulsion between interlayer anions. Therefore, in 35F, NO_3^- ions were stabilized by the moderate balance between interactions with the brucite-like layer and the steric and electrostatic repulsion between the interlayer NO_3^- ions.

Finally, the XRD patterns of all samples after the SO_4^{2-}-exchange test are shown in Figure 6c. Two new diffraction lines were observed at lower 2θ values of ~8.7 Å, in addition to the original (003) and (006) diffraction lines. At the same time, the positions of these original diffraction lines shifted toward a higher 2θ value of ~7.8 Å, indicating that large sulfate ions were intercalated to expand the interlayer distance and push against neighboring layers, resulting in a reduction of the interlayer distance. Two trends in line positions can be seen in Figure 6c: the position of a new diffraction line near the (003) line shifted to a higher 2θ value as the Mg/Al ratio increased and the diffraction line intensity decreased in the XRD patterns of the F-LDHs. For the first trend, when the Mg/Al ratio was lower, a higher number of SO_4^{2-} ions in interlayer space induced strong electrostatic repulsion, leading to the expansion of the interlayer distance. The second trend corresponds to a significant decrease in K_d values among the F-LDHs, possibly because the narrower interlayer space prevents SO_4^{2-} ions from intercalating, which is a steric effect. This trend is consistent with the K_d result.

The results of the ion-exchange tests demonstrate that the compatibility of the Mg/Al ratio and fluorine substitution in LDHs significantly changed the interlayer structure to sterically inhibit large SO_4^{2-} ions from intercalating. However, the key factor in describing the difference between the affinities for F^- and NO_3^- ions remains unclear at this point.

To identify the local structure of LDHs, FT-IR and Raman spectroscopic analysis were carried out. Using the representatives 35 and 35F, a band corresponding to the δ mode of O−H groups was observed at around 600 cm^{-1}, a strong ν_3 mode at 1360 cm^{-1} with a weak ν_2 mode at 830 cm^{-1} for the CO_3^{2-} ions, and a water-bending mode around 1635−1650 cm^{-1} in the low-wavenumber region in Figure 7A-a and -i.[21,38−40] Here, all spectra were normalized along with the intensity of the δ modes of OH groups. The infrared feature at 1360 cm^{-1} is different from that at 1400 cm^{-1}, which can be attributed to free CO_3^{2-} ions, indicating that CO_3^{2-} ions existed as interlayer anions. In the high-wavenumber region, an intense band centered at approximately 3400 cm^{-1} appears because of the stretching modes of hydroxyl groups belonging to the

DOI: 10.1021/acs.inorgchem.9b01552
Inorg. Chem. XXXX, XXX, XXX−XXX

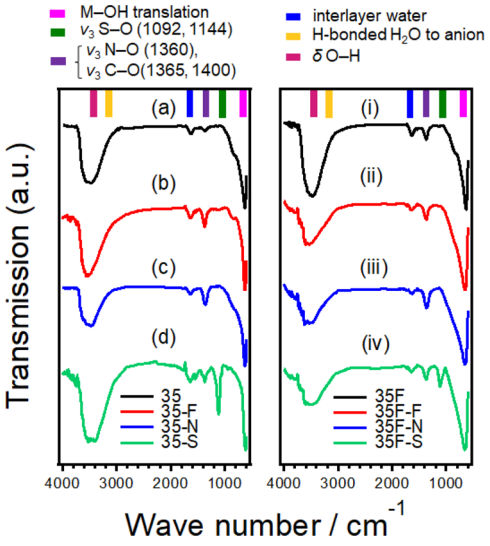

Figure 7. FT-IR spectra of LDHs: (a) 35, (b) 35-F, (c) 35-N, (d) 35-S, (i) 35F, (ii) 35F-F, (iii) 35F-N, and (iv) 35F-S.

brucite-like layer and water molecules.[19,23,24,35−37] It was difficult to identify the bands as they overlapped with each other. The bands at ∼3380 cm^{-1} are attributed to water coordinated to the brucite-like layer—M_3OH units (M = Al or Mg)—and the bands at 3480 cm^{-1} are attributed to water between the brucite-like layers, as reported in previous studies.[37] In addition, the interaction between interlayer water molecules and the carbonate ions is reflected by the feature around 2800−3100 cm^{-1} in the OH stretching region of the infrared spectrum.[19,24,35−38] This band can be attributed to the bridging mode between H_2O and CO_3^{2-} ions. Only a very limited number of Raman studies have been reported so far on interlayer carbonates in LDHs. Figure S7 shows a very strong ν_1 mode at 1061 cm^{-1} in the Raman spectrum. The features at around 470 and 549 cm^{-1} can be attributed to the Mg−O and Al−O symmetric stretching vibrations, respectively.[35,36,38−40]

We renamed 35 after the ion-exchange tests of F^-, NO_3^-, and SO_4^{2-} ions as 35-F, 35-N, and 35-S, respectively, and the infrared spectra of the post-test LDHs are shown in panels b−d of Figure 7, respectively. The infrared spectra of 35F-F, 35F-N, and 35F-S obtained after ion-exchange tests of 35F are shown in panels ii−iv of Figure 7, respectively. Notably, the peak intensity of the infrared spectra of 35F near 600 cm^{-1} was slightly red-shifted compared to that of 35. Furthermore, those of 35F-F, 35F-N, and 35F-S at around 600 cm^{-1} show band broadening and a slight red shift when compared to the data of 35F, which correspond to the decreasing intensity of the spectrum attributed to interlayer water around 1635−1650 and 3480 cm^{-1}. Similar behavior was reported in an earlier study, in which a decreasing Mg/Al ratio in LDHs led to decreasing interlayer water.[21] The red shift suggests that a higher vibrational energy might have resulted from the weakened interactions between the interlayer anion and the brucite-like layer, while the broadening implies that the brucite-like layer had a disturbed structure. In the case of 35, after F^-- and SO_4^{2-}-exchange tests, the increment of interlayer water compared to the sample after NO_3^--exchange tests could be observed probably because the higher polarity of F^- and SO_4^{2-} ions attracted water surrounding them even in interlayer space. However, for 35F LDHs there was hardly any difference in the behavior of interlayer water after ion-exchange tests in all samples.

Other than the results regarding interlayer water, the infrared and Raman spectra of 35-F and 35F-F showed little difference before and after the ion-exchange test. Even after the F^- ion-exchange test, some amount of CO_3^{2-} ions remained in the LDHs, as indicated in Figure 7 and Figure S7; the same was observed in the samples after the NO_3^-- and SO_4^{2-}-exchange tests. An intensive sharp feature of the ν_3 mode was observed at 1384 cm^{-1}, and one was observed for the ν_2 mode at 830 cm^{-1} in the Raman spectra of 35-N and 35F-N.[40−44] In the IR spectrum, it is difficult to identify the coordination state of NO_3^- ions, unlike that of CO_3^{2-} ions, because there is only a small difference between the positions of peaks corresponding to free and interlayer NO_3^- ions and small H_2O−NO_3^- ion interactions. This information can be more easily obtained from the Raman spectra. On the basis of the peak corresponding to free NO_3^- ions at 690 cm^{-1}, the Raman peak of the ν_4 mode at 712 cm^{-1} in Figure S7 indicates that the NO_3^- ions resided in the interlayer space in both 35-N and 35F-N.[40]

The infrared spectra of 35-S and 35F-S in panels d and iv of Figure 7 show a strong ν_3 mode at 1126 cm^{-1} and a very weak ν_1 mode at 981 cm^{-1}.[19,24,35−39] The Raman spectra in Figure S4 can be characterized by a very strong ν_1 mode at 982 cm^{-1} and ν_2 and ν_4 modes at 453 and 611 cm^{-1}, respectively.[19,24,38,40−42] In addition, the ν_3 mode of a broad band can be seen around 1134 cm^{-1}, along with other features at 980 and 990 cm^{-1}, which are assigned to the nardite and SO_4^{2-} ions, respectively.[45] As reported in an earlier paper, when sulfate is incorporated into the interlayer space, the infrared ν_2 mode at 500 cm^{-1} might become inactive, while the ν_1 mode is activated.[40] However, it was difficult to identify the position of SO_4^{2-} ions in our results because of the overlapping Raman peaks. The results of FT-IR and Raman spectroscopy confirmed that the inclusion of various anions into the interlayer space of LDHs should affect not only the interlayer distance but also the microscale behavior of the brucite-like layer and interlayer water. However, these two kinds of behavior are difficult to distinguish in the FT-IR spectra.

In FT-IR spectroscopy, H_2O−OH stretching vibrations are very intense because of the large change in dipole moment, which makes it difficult to deconvolute the spectra and distinguish between the signals corresponding to hydroxyl groups of water and the metal hydroxides. Water is, on the other hand, a very weak Raman scatterer, and the OH stretching modes are not as intense in the Raman spectrum; however, researchers traditionally focus on the OH stretching region at 3000−3800 cm^{-1} to reveal the dynamic structure of water, such as ice-like water at low temperature and in the interlayer space in clay and minerals. The Raman peaks of 35 and 35F are indicated in Figure 8. The broad Raman peak observed in the 3000−3800 cm^{-1} range was deconvoluted into six subpeaks located at around 3270, 3400, 3520, 3590, 3640, and 3680 cm^{-1}.[41,42] The former three subpeaks are assigned to interlayer water, and the latter three subpeaks are assigned to OH stretching modes belonging to the brucite-like layer with different coordination states. In particular, among the three former subpeaks, the peak at around 3270 cm^{-1} corresponds to interlayer water coordinated to the brucite-like layer, and those at around 3400 and 3520 cm^{-1} correspond to two types of water coordinated to water in the interlayer space. However, completely assigning the OH stretching modes belonging to

DOI: 10.1021/acs.inorgchem.9b01552
Inorg. Chem. XXXX, XXX, XXX−XXX

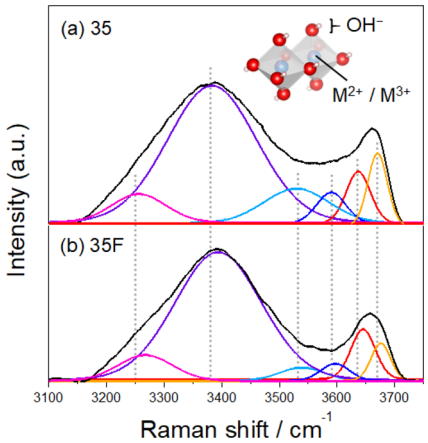

Figure 8. Raman spectra of LDHs in the range from 3100 to 3750 cm^{-1}: (a) 35 and (b) 35-F.

the brucite-like layer seems difficult as the peak in this region was convoluted from two or three peaks owing to intercalated species.[41,42] In a previous report, the feature at around 3590 cm^{-1} was attributed to Al−OH stretching vibrations, and the one at around 3640 cm^{-1} was attributed to Mg−OH stretching vibrations.[41,42] However, when the peak in this region was deconvoluted into three peaks, a detailed peak assignment was avoided. Important evidence for revealing the local structure of LDHs has been acquired using ^{1}H solid-state NMR spectroscopy.[43−45] Peng and co-workers showed that Mg−Al LDH with a low Al content (a composition similar to that in our study) has Mg_2Al−OH and Mg_3−OH species, although the Raman spectroscopic results in their study clearly showed three kinds of OH stretching modes in this region.[44] In addition, $MgAl_2$−OH existed only in Al-rich LDHs.[45] According to vibrational theory, the OH stretching modes of species with weaker hydrogen bonding with anions and water should lie in the higher-wavenumber region. On the basis of these findings, the peaks at around 3590, 3640, and 3680 cm^{-1} are attributed to Mg_2Al−OH, Mg_3−OH, and Mg_3−OH species, respectively, being free or weakly interacting with anions and/or interlayer water. Mg_2Al−OH and the former Mg_3−OH are believed to interact with anions and water through hydrogen bonding, considering spatial charge compensation.

As a result of deconvolution along with the discussion presented above, all subpeaks for 35F clearly shifted to higher wavenumber relative to those of 35, as shown in Figure 8. The shift observed in the interlayer water region at 3150−3600 cm^{-1} corresponds to a decreased amount of hydrogen bonding, implying the decreased volume of the water network in the interlayer space. This finding is consistent with XRD results, which revealed that the interlayer space in F-LDHs was smaller than that in the original LDHs. Thus, steric effects of the shrunken interlayer space in 35F possibly arose from the structural distortion of interlayer water, which was triggered by weakened hydrogen bonding with OH structural groups in F-LDHs. For the peaks of the OH structural groups at 3550−3700 cm^{-1}, the shift to higher wavenumber can be interpreted as weakened hydrogen bonding interactions between the OH structural groups and both the anions and the interlayer water molecules. This behavior presumably results from the decreased polarity of the O−H bonding, which occurs because of the strong electronegativity of the fluorine atoms incorporated into the Al and Mg octahedra in the brucite-like layer. This finding is consistent with the slight red shift in Mg−O and Al−O symmetric stretching vibrations, as observed in the FT-IR spectra. Therefore, fluorine substitution is concluded to affect not only interlayer water but also intermolecular interactions by causing slight structural changes to the brucite-like layer. Possible interactions in the interlayer space are assumed to be Coulombic forces, hydrogen bonding, and van der Waals forces. In the case of the original LDHs, both Coulombic forces and hydrogen bonding are considered to be predominant, as previously demonstrated. Thus, LDHs exhibited a high affinity for SO_4^{2-} and F^- ions owing to the high charge density and hydrogen bonding. On the other hand, in F-LDHs, van der Waals forces are assumed to be predominant owing to the decreased hydrogen bonding interactions. In this regard, it is reasonable that F-LDHs exhibited a higher affinity for NO_3^- ions than for F^- ions from the viewpoint of van der Waals interactions, because the former have a higher molecular weight than the latter. They also exhibited a higher affinity for NO_3^- ions than for SO_4^{2-} ions owing to steric effects. Note that Coulombic forces are critical from the viewpoint of charge compensation. Therefore, our results suggest for the first time that tuning the hydrogen bonding and van der Waals forces significantly changes the affinity for particular ions in interlayer space of inorganic ion exchangers.

CONCLUSION

We attempted to prepare fluorine-substituted Mg−Al LDHs (F-LDHs) with different Mg/Al ratios by replacing OH structural groups belonging to the host layer of LDHs with fluorine atoms. The affinity of LDHs for various anions was investigated. Only F-LDHs with Mg/Al ratios of 3.5 exhibited higher affinity, especially for NO_3^- ions, where the affinity decreased in the following order: $NO_3^- > HPO_4^{2-} > Br^- > F^- > SO_4^{2-} > I^-$. The separation factors with respect to both NO_3^-/F^- and NO_3^-/SO_4^{2-} were higher than that of LDHs with other compositions by 1 order of magnitude. Raman spectroscopy above 3000 cm^{-1} revealed that the fluorine substitution of LDHs significantly changed the hydrogen bonding nature in the interlayer space. Highly electronegative fluorine atoms significantly weakened the hydrogen bonding interactions between the OH structural groups and both the water molecules and anions in the interlayer space, because steric effects were induced by the shrunken interlayer space and van der Waals forces were revealed to be the predominant interactions with anions. Therefore, in F-LDHs, the highest affinity was observed for NO_3^- ions. Finally, we believe that this work on the control of interlayer nanospace in LDHs will contribute not only to their use as ion exchangers but also in ion conduction and as photo- and electrocatalysts by tuning their electronic structure and surface properties.

ASSOCIATED CONTENT

Supporting Information

The Supporting Information is available free of charge at https://pubs.acs.org/doi/10.1021/acs.inorgchem.9b01552.

Experimental procedure, compositional information about as-prepared LDHs that were obtained by ICP-OES and EDS analysis, ^{19}F NMR spectra (30 kHz) of 35F and 40F recorded with an internal reference (PTFE), dependence of K_d value on the ionic radii of target anions, ion-exchange ratio in the total amount of

DOI: 10.1021/acs.inorgchem.9b01552
Inorg. Chem. XXXX, XXX, XXX−XXX

anion removed, dependence of SF values on F substitution ratio, and Raman spectra in the low-wavenumber region (PDF)

AUTHOR INFORMATION

Corresponding Author

*E-mail: teshima@shinshu-u.ac.jp.

ORCID

Tomohito Sudare: 0000-0002-9060-4291
Nicolas Louvain: 0000-0001-8727-6832
Fumitaka Hayashi: 0000-0002-4494-739X
Katsuya Teshima: 0000-0002-5784-5157

Notes

The authors declare no competing financial interest.

ACKNOWLEDGMENTS

This work was partially supported by the "A Shinshu-Method for Regional Innovation Ecosystem by Industrial Implementation of Innovative Inorganic Crystal Material Technology" project of the "Program on Regional Innovation and Ecosystem Formation" of the Ministry of Education, Culture, Sports, Science and Technology (MEXT), Japan, the Matching Planner Program of the Japan Science and Technology Agency (JST), and Environment Research and Technology Development Fund 5RF-1902 of the Environmental Restoration and Conservation Agency of Japan. In addition, the authors appreciate the helpful guidance of Dr. Tomohiko Okada, associate professor of Shinshu University, with the NMR measurements.

ABBREVIATIONS

ATR, attenuated total reflection; BET, Brunauer−Emmett−Teller; EDS, energy-dispersive X-ray spectrometry; F-LDH, fluorine-substituted layered double hydroxide; FE-SEM, field-emission scanning electron microscopy; FT-IR, Fourier transform infrared; IC, ion chromatography; LDH, layered double hydroxide; NMR, nuclear magnetic resonance; MAS, magic angle spinning; SF, separation factor; XPS, X-ray photoelectron spectroscopy; XRD, X-ray diffraction.

REFERENCES

(1) Futamura, R.; Iiyama, T.; Takasaki, Y.; Gogotsi, Y.; Biggs, M. J.; Salanne, M.; Ségalini, J.; Simon, P.; Kaneko, K. Partial breaking of the Coulombic ordering of ionic liquids confined in carbon nanopores. *Nat. Mater.* **2017**, *16*, 1225−1232.

(2) Fujimori, T.; Morelos-Gomez, A.; Zhu, Z.; Muramatsu, H.; Futamura, R.; Urita, K.; Terrones, M.; Hayashi, T.; Endo, M.; Young Hong, S.; Chul Choi, Y.; Tomanek, D.; Kaneko, K. Conducting linear chains of sulphur inside carbon nanotubes. *Nat. Commun.* **2013**, *4*, 2162.

(3) Kitagawa, S.; Kitaura, R.; Noro, S. Functional Porous Coordination Polymers. *Angew. Chem., Int. Ed.* **2004**, *43*, 2334.

(4) Zhao, Y.; Zhao, Y.; Waterhouse, G. I. N.; Zheng, L.; Cao, X.; Teng, F.; Wu, L. Z.; Tung, C. H.; O'Hare, D.; Zhang, T. Layered-Double-Hydroxide Nanosheets as Efficient Visible-Light-Driven Photocatalysts for Dinitrogen Fixation. *Adv. Mater.* **2017**, *29* (42), 1703828.

(5) Wang, Q.; O'Hare, D. Recent Advances in the Synthesis and Application of Layered Double Hydroxide (LDH) Nanosheets. *Chem. Rev.* **2012**, *112* (7), 4124−4155.

(6) Miyata, S. Anion-exchange Properties of hydrotalcite-like Compounds. *Clays Clay Miner.* **1983**, *31* (4), 305−311.

(7) Puerta-Falla, G.; Balonis, M.; Falzone, G.; Bauchy, M.; Neithalath, N.; Sant, G. Monovalent Ion Exchange Kinetics of Hydrated Calcium-Alumino Layered Double Hydroxides. *Ind. Eng. Chem. Res.* **2017**, *56* (1), 63−74.

(8) Tezuka, S.; Chitrakar, R.; Sonoda, A.; Ooi, K.; Tomida, T. Nitrate Ion-Sieve Properties of Layered Double Hydroxides. *Chem. Lett.* **2003**, *32* (8), 722−723.

(9) Das, J.; Patra, B. S.; Baliarsingh, N.; Parida, K. M. Adsorption of Phosphate by Layered Double Hydroxides in Aqueous Solutions. *Appl. Clay Sci.* **2006**, *32* (3−4), 252−260.

(10) Ma, L.; Islam, S. M.; Xiao, C.; Zhao, J.; Liu, H.; Yuan, M.; Sun, G.; Li, H.; Ma, S.; Kanatzidis, M. G. Rapid Simultaneous Removal of Toxic Anions $[HSeO_3]^-$, $[SeO_3]^{2-}$, and $[SeO_4]^{2-}$, and Metals Hg^{2+}, Cu^{2+}, and $Cd^{2+}$by MoS_4^{2-}Intercalated Layered Double Hydroxide. *J. Am. Chem. Soc.* **2017**, *139* (36), 12745−12757.

(11) Kameda, T.; Kondo, E.; Yoshioka, T. Preparation of Mg-Al Layered Double Hydroxide Doped with Fe^{2+} and Its Application to Cr(VI) Removal. *Sep. Purif. Technol.* **2014**, *122*, 12−16.

(12) Ookubo, A.; Ooi, K.; Hayashi, H. Preparation and Phosphate Ion-Exchange Properties of a Hydrotalcite-like Compound. *Langmuir* **1993**, *9* (5), 1418−1422.

(13) Ma, B.; Fernandez-Martinez, A.; Grangeon, S.; Tournassat, C.; Findling, N.; Carrero, S.; Tisserand, D.; Bureau, S.; Elkaïm, E.; Marini, C.; Aquilanti, G.; Koishi, A.; Marty, N. C. M.; Charlet, L. Selenite Uptake by Ca-Al LDH: A Description of Intercalated Anion Coordination Geometries. *Environ. Sci. Technol.* **2018**, *52* (3), 1624−1632.

(14) Hibino, T. Anion Selectivity of Layered Double Hydroxides: Effects of Crystallinity and Charge Density. *Eur. J. Inorg. Chem.* **2018**, *2018* (6), 722−730.

(15) Bontchev, R. P.; Liu, S.; Krumhansl, J. L.; Voigt, J.; Nenoff, T. M. Synthesis, Characterization, and Ion Exchange Properties of Hydrotalcite $Mg_6Al_2(OH)_{16}(A)x(A')_{2-x}$, $4H_2O(A,A')C^{l-}$, Br^-, I^-, and NO_3^-, $2H_2O$) Derivatives. *Chem. Mater.* **2003**, *15* (19), 3669−3675.

(16) Ivánová, D.; Albert, P.; Kavuličová, J. Nitrate Removal from Model Aqueous Solutions and Real Water by Calcined Mg/Al Layered Double Hydroxides. *Appl. Clay Sci.* **2018**, *152*, 65−72.

(17) Bhatnagar, A.; Sillanpää, M. A Review of Emerging Adsorbents for Nitrate Removal from Water. *Chem. Eng. J.* **2011**, *168* (2), 493−504.

(18) Shrimali, M.; Singh, K. P. New Methods of Nitrate Removal from Water. *Environ. Pollut.* **2001**, *112* (3), 351−359.

(19) Costa, D. G.; Rocha, A. B.; Souza, W. F.; Chiaro, S. S. X.; Leitão, A. A. Comparative Structural, Thermodynamic and Electronic Analyses of ZnAlAn − Hydrotalcite-like Compounds (A^-: Cl−, F^-, Br^-, OH^-, CO_3^{2-} or NO3$^-$): An Ab Initio Study Applied Clay Science Comparative Structural, Thermodynamic and Electronic Analy. *Appl. Clay Sci.* **2012**, *56*, 16−22.

(20) Hyman, R. J. Access to Library Collections. *An Inquiry into Validity Direct Shelf Approach, with Specific Reference to Brows*; Screcrow Press. Inc.: Metuchen, NJ, 1972.

(21) Xu, Z. P.; Zeng, H. C. Abrupt Structural Transformation in Hydrotalcite-like Compounds $Mg_{1-x}Al_x(OH)_2(NO_3)_x{\cdot}nH_2O$ as a Continuous Function of Nitrate Anio. *J. Phys. Chem. B* **2001**, *105* (9), 1743−1749.

(22) Nieto-Malagón, G.; Cuautli, C.; Ireta, J. Interlaminar Anionic Transport in Layered Double Hydroxides: Estimation of Diffusion Coefficients. *J. Phys. Chem. C* **2018**, *122* (1), 171−176.

(23) Bezen, M. C. I.; Breitkopf, C.; Lercher, J. A. Influence of Fluoride Anions on the Acid-Base Properties of Mg/Al Mixed Oxides. *ACS Catal.* **2011**, *1* (10), 1384−1393.

(24) Sanjuan, B.; Michard, G. Aluminum Hydroxide Solubility in Aqueous Solutions Containing Fluoride Ions at 50°C. *Geochim. Cosmochim. Acta* **1987**, *51* (7), 1823−1831.

(25) Sakida, S.; Shojiya, M.; Kawamoto, Y. 27Al MAS NMR study on anion coordination around Al3+ in AlF_3-BaF_2-$BaCl_2$-CaF_2-YF_3-EuF_3 glasses. *J. Fluorine Chem.* **2000**, *106* (2), 127−131.

(26) Lacassagne, V.; Bessada, C.; Florian, P.; Bouvet, S.; Ollivier, B.; Coutures, J.-P.; Massiot, D. Structure of High-Temperature NaF-

DOI: 10.1021/acs.inorgchem.9b01552
Inorg. Chem. XXXX, XXX, XXX−XXX

AlF_3-Al_2O_3 Melts: A Multinuclear NMR StudD. *J. Phys. Chem. B* **2002**, *106*, 1862−1868.
(27) Chan, J. C. C.; Eckert, H. High-resolution 27Al−19F solid-state double resonance NMR studies of AlF_3−BaF_2−CaF_2 glasses. *J. Non-Cryst. Solids* **2001**, *284* (1−3), 16−21.
(28) Scholz, G.; Kemnitz, E. Mechanochemical synthesis of AlF_3 with NH_4F as fluorinating agent − Does it work? *Solid State Sci.* **2009**, *11*, 676.
(29) Body, M.; Silly, G.; Legein, C.; Buzare, J.-Y. Correlation between 19F Environment and Isotropic Chemical Shift in Barium and Calcium Fluoroaluminates. *J. Phys. Chem. B* **2005**, *109*, 10270−10278.
(30) Bureau, B.; Silly, G.; Emery, J.; Buzare, J.-Y. Superposition model for 19F isotropic chemical shift in ionic fluorides: from basic metal fluorides to transition metal fluoride glasses. *Chem. Phys.* **1999**, *249*, 89.
(31) Hagenmuller, P. *Inorganic Solid Fluorides*; Academic Press, Inc., 1985.
(32) Sadoc, A.; Body, M.; Legein, C.; Biswal, M.; Fayon, F.; Rocquefelte, X.; Boucher, F. NMR parameters in alkali, alkaline earth and rare earth fluorides from first principle calculations. *Phys. Chem. Chem. Phys.* **2011**, *13* (41), 18539−18550.
(33) Bessada, C.; Anghel, E. M. ^{11}B, ^{23}Na, ^{27}Al, and ^{19}F NMR Study of Solid and Molten Na_3AlF_6−$Na_2B_4O_7$. *Inorg. Chem.* **2003**, *42* (12), 3884−3890.
(34) Bessada, C.; Lacassagne, V.; Massiot, D.; Florian, P.; Coutures, J. P.; Robert, E.; Gilbert, B. Structural and dynamic approaches of molten salts by high temperature spectroscopies. *Z. Naturforsch., A: Phys. Sci.* **1999**, *54* (2), 162−166.
(35) Wuttke, S.; Coman, S. M.; Scholz, G.; Kirmse, H.; Vimont, A.; Daturi, M.; Schroeder, S. L. M.; Kemnitz, E. Novel Sol−Gel Synthesis of Acidic $MgF_{2-x}(OH)_x$ Materials. *Chem. - Eur. J.* **2008**, *14*, 11488.
(36) Zheng, A.; Liu, S.-B.; Deng, F. ^{19}F Chemical Shift of Crystalline Metal Fluorides: Theoretical Predictions Based on Periodic Structure Models. *J. Phys. Chem. C* **2009**, *113* (33), 15018−15023.
(37) Du, L.-S.; Samoson, A.; Tuherm, T.; Grey, C. P. $^{19}F/^{23}Na$ Double Resonance MAS NMR Study of Oxygen/Fluorine Ordering in the Oxyfluoride $Na_5W_3O_9F_5$. *Chem. Mater.* **2000**, *12* (12), 3611−3616.
(38) Serna, C. J.; Rendon, J. L.; Iglesias, J. E. Crystal-Chemical Study of Layered $[A1_2Li(OH)_6]+X^-$ nH_2O. *Clays Clay Miner.* **1982**, *30* (3), 180−184.
(39) Kloprogge, J. T.; Hickey, L.; Frost, R. L. FT-Raman and FT-IR Spectroscopic Study of Synthetic Mg/Zn/Al-Hydrotalcites. *J. Raman Spectrosc.* **2004**, *35* (11), 967−974.
(40) Kloprogge, J. T.; Wharton, D.; Hickey, L.; Frost, R. L. Infrared and Raman Study of Interlayer Anions CO_3^{2-}, NO_3^-, SO_4^{2-} and ClO_4^- in Mg/Al Hydrotalcite. *Am. Mineral.* **2002**, *87* (3), 623−629.
(41) Palmer, S. J.; Nguyen, T.; Frost, R. L. Synthesis and Raman Spectroscopic Characterisation of Hydrotalcite with CO_3^{2-} and $(VO_3)^-$ Anions in the Interlayer. *J. Raman Spectrosc.* **2007**, *38*, 1602−1608.
(42) Palmer, S. J.; Frost, R. L.; Ayoko, G.; Nguyen, T. Synthesis and Raman Spectroscopic Characterisation of Hydrotalcite with CO_3^{2-} and $(MoO_4)^{2-}$ Anions in the Interlayer. *J. Raman Spectrosc.* **2008**, *39*, 395−401.
(43) Sideris, P. J.; Nielsen, U. G.; Gan, Z.; Grey, C. P. Mg/Al Ordering in Layered Double Hydroxides Revealed by Multinuclear NMR Spectroscopy. *Science* **2008**, *321*, 113−117.
(44) Yu, G.; Shen, M.; Wang, M.; Shen, L.; Dong, W.; Tang, S.; Zhao, L.; Qi, Z.; Xue, N.; Guo, X.; Ding, W.; Hu, B.; Peng, L. Probing Local Structure of Layered Double Hydroxides with ^1H Solid-State NMR Spectroscopy on Deuterated Samples. *J. Phys. Chem. Lett.* **2014**, *5*, 363−369.
(45) Cadars, S.; Layrac, G.; Gerardin, C.; Deschamps, M.; Yates, J. R.; Tichit, D.; Massiot, D. Identification and Quantification of Defects in the Cation Ordering in Mg/Al Layered Double Hydroxides. *Chem. Mater.* **2011**, *23*, 2821−2831.

DOI: 10.1021/acs.inorgchem.9b01552
Inorg. Chem. XXXX, XXX, XXX−XXX